Mechanistic studies on the alcoholysis and aminolysis of [(MeZn)₂{μ-N(H)tBu}{μ-N(CH₂Py)₂}]

Marcel Kahnes [a], Julia Richthof [a], Helmar Görls [a], Daniel Escudero [b], Leticia González [b,*],
Matthias Westerhausen [a,*]

[a] Institut für Anorganische und Analytische Chemie, August-Bebel-Str. 2, 07743 Jena, Germany
[b] Institut für Physikalische Chemie, Helmholtzweg 4, 07743 Jena, Germany

ARTICLE INFO

ABSTRACT

The reaction of bis(2-pyridylmethyl)amine (**II**) with t-butylamine and dimethylzinc gives the heteroleptic [(MeZn)₂{μ-N(H)tBu}{μ-N(CH₂Py)₂}] (**1**). Stoichiometric alcoholysis of **1** with methanol leads to the exchange of the μ-N(H)tBu moiety. Almost quantitatively the corresponding methoxide [(MeZn)₂(μ-OMe){μ-N(CH₂Py)₂}] (**2**) is formed. Alternatively bis(alkylzinc)methoxide-bis(2-pyridylmethyl)amides (Alkyl = methyl (**2**), bis(trimethylsilyl)methyl (**3**)) are also accessible by direct zincation of bis(2-pyridyl-methyl)amine (**II**) and methanol with dialkylzinc regardless of the bulkiness of the alkyl groups. Extensive DFT calculations on the alcoholysis mechanism reveal the preferential insertion of methanol into a zinc amide bond rather than the cleavage of zinc carbon bonds. An intermediate with a Zn[μ-(MeO···H···NHR)]Zn functionality is predicted. Aminolyis of **1** with t-butylamine leads to intermediates with Zn[μ-(RNH···H···NHR)]Zn functionalities, respectively. We were able to detect the latter by ^{1}H NMR spectroscopy. The aminolysis of **1** with an excess of phenylamine results in a partial decomposition of the complex leading to the hexanuclear amide [{Zn(μ-N(H)Ph)}{MeZn(μ-N(H)Ph)}₂{μ-N(CH₂Py)}]₂ (**4**). Compound **2** is able to cleave silicon grease when dissolved in t-butylamine yielding [(MeZn)₂{μ-N(CH₂Py)₂}₂Zn{μ-(OMe₂Si)₂O}] (**5**). The X-ray structures of complexes **1–5** are discussed.

1. Introduction

Playing an essential role in protein degradation as well as in metabolic cycles binuclear zinc hydrolases are widely spread among both eucaryotes and procaryotes. As a common feature they display a Zn–OH–Zn bridge in the active site [1] and a bridging carboxylate ligand as backbone, keeping the zinc ions in fixed positions. Additional ligands which bind via a nitrogen or an oxygen donor saturate the coordination sphere (Fig. 1).

Insight into the chemical processes taking place at the active side of the metallo-enzyme can be obtained by investigating the enzymatic system itself or by choosing a biomimetic model, which can be studied kinetically or with quantum chemical methods [2]. A comprehensive summary in the field of synthetic enzyme analogues was recently provided by Parkin [3].

As advantageous ligands in bioinorganic chemistry (2-pyridyl-methyl)amine (2-picolylamine) and their substitution products are a subject of great interest for the synthesis of biomimetic models [3,4]. In recent years our group has studied their reaction

behavior towards dialkylzinc compounds in order to obtain multi-nuclear zinc complexes. (2-Pyridylmethyl)amine reacts with dialkylzinc to form the corresponding alkylzinc (2-pyridyl-methyl)amide which, depending on the size of the zinc bound alkyl substituent, crystallizes either as dimer or trimer [5]. Zincation of N-silylated (2-pyridylmethyl)amine (**I**) with alkylzinc reagents yields the dimeric silylamide (**III**). Addition of an excess of dimethylzinc to complex **III** results in an oxidative C–C coupling reaction giving dinuclear **IV**. In the course of the reaction metallic zinc precipitates and methane is liberated [6,7] (Fig. 2). The reaction of dipicolylamine (**II**) with equimolar amounts of dialkylzinc leads to the formation of dimeric alkylzinc dipicolylamide regardless of the steric bulk of the alkyl substituent. In the solid state only one pyridyl group of each ligand coordinates to the zinc ion [8,9], however, in solution both pyridyl groups are equivalent on the NMR time scale due to exchange processes. In this case additional dimethylzinc does not lead to oxidative C–C coupling reactions, but metallation of one methylene group, resulting in complex **VII**, is observed. Thermolysis of **V** at approximately 300 °C reveals a novel and completely unexpected reaction behavior of the ambidentate dipicolylamide. In a dehydrogenation reaction zinc bis[1,3-di(2-pyridyl)-2-azapropenide] (**VIII**) is formed, which sublimates as gold-shining crystals [10]. Although the reaction mechanism remains unknown compound **VII** is considered as key intermediate

* Corresponding authors. Tel.: +49 (0)3641 9 48360; fax: +49 (0)3641 9 4830 (L. González); tel.: +49 (0)3641 9 48110; fax: +49 (0)3641 9 48102 (M. Westerhausen).
E-mail addresses: leticia.gonzalez@uni-jena.de (L. González), m.we@uni-jena.de (M. Westerhausen).
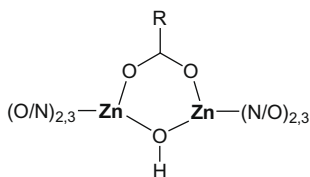
Fig. 1. Common structural motif for the active side of many zinc hydrolases.

on the way to complex **VIII**. A similar behavior is observed for the dibenzylamido anion (($PhCH_2)_2N^-$) which, mediated by PMDETA (($Me_2NCH_2CH_2)_2NMe$) solvated Li^+, Na^+ and K^+ counterions, readily converts to the corresponding 1,3-diphenyl-2-azapropenide. In this case the azaallyl conversion can be explained as a two-step process consisting of a β-elimination of a metal hydride followed by hydride metallation of the produced imine $PhCH_2N = C(H)Ph$ [11].

Exposure of a concentrated solution of **VI** to air leads to a slow partial hydrolysis resulting in the formation of the hydroxide com-

plex **IX** (Fig. 3), in which the dipicolylamide serves as tetradentate backbone. Though being significantly more acidic, an amine is eliminated in the course of hydrolysis, whereas the Zn–C bond remains intact. Extensive DFT calculations at the B3LYP/lanl2dz level of theory confirm the mode of action of hydrolysis reasoned by the preferential formation of a relatively stable intermediate with a $Zn[\mu\text{-}(HO\cdots H\cdots NR)]Zn$ moiety [9].

The existence of $Zn[\mu\text{-}(HO\cdots H\cdots OH)]Zn$ fragments has already been shown experimentally by several solid-state structures of biomimetic zinc complexes [12]. Kinetic investigations on binuclear zinc complexes show that such H_3O_2 species are intrinsically more reactive than μ-OH units [12,13]. Therefore the formation of H_3O_2 functionalities is discussed as an important step in the mode of action of binuclear zinc hydrolases [14] also being demonstrated by a recent DFT study [15].

In the course of this work we like to expand the concept of the hydrolysis of alkylzinc dipicolylamides in order to obtain new binuclear zinc complexes with a bridging μ-OR moiety. Furthermore, we investigated the generality of the occurence of $Zn[\mu\text{-}(X\cdots H\cdots Y)]Zn$ (X = O, N; Y = N) according to biomimetic models.
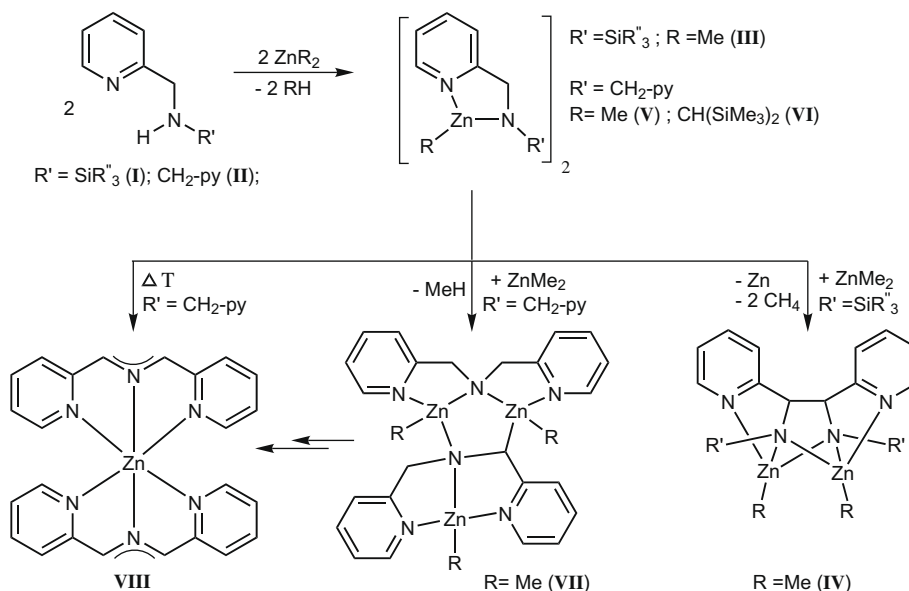

Fig. 2. Reactivity of N-substituted 2-pyridylmethylamines towards dialkylzinc reagents.
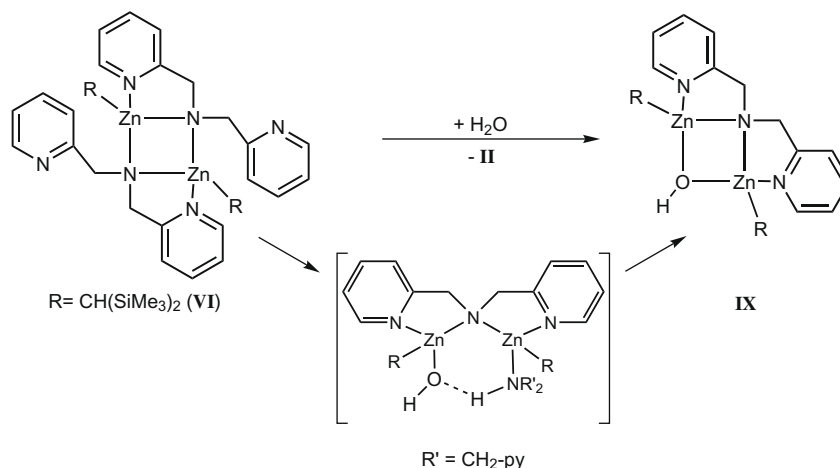

Fig. 3. Hydrolysis of **VI**.

2. Results and discussion

2.1. Synthesis and characterization of bis(methylzinc)**t**-butylamide-bis(2-pyridylmethyl)amide (**1**)

In order to gain the ability of a kinetically controlled hydrolysis the heteroleptic zinc amide **1** was synthesized with a chelating dipicolylamide as backbone and a bridging *t*-butylamide as the reactive site. Direct metallation of stoichiometric amounts of *t*-butylamine and dipicolylamine (**II**) with dimethylzinc in toluene leads to the desired complex which crystallizes with tetra-coordinated zinc atoms (see Fig. 4).

The molecular structure of **1** (Fig. 5) shows a Zn_2N_2 unit as central structural element with different endocyclic Zn1/2–N2 and Zn1/2–N4 bond lengths. The latter are slightly shorter (∼5 pm) than the Zn1/2–N2 bonds (209.9 and 208.8 pm) but still slightly elongated compared to those reported for trimeric [EtZnNH^{t}Bu]$_3$ (202.0 pm) [16]. This effect is a consequence of the enlarged coordination sphere of zinc in compound **1**. The exocyclic Zn–N$_{pyridyl}$ bonds (216.3 and 219.0 pm) are somewhat larger than the Zn1/2–N2 distances due to reduced electrostatic attraction. Nevertheless, those bond lengths are very similar to those of complex **V** (Zn–N$_{py}$ = 217.6 pm; Zn–(μ-N) = 210.3 pm) [9]. The Zn1–C13 bond length in **1** (198.2 pm) is comparable to the one reported for **V** (199.0 pm) but slightly elongated compared to dimethylzinc (195.5 pm) with a metal atom of the coordination number of two [17]. The Zn_2N_2 ring is significantly folded (∼28.2°) and shows a transannular non-bonding Zn1 · · · Zn2 distance of 285.8 pm.

2.2. Partial methanolysis of **1** and the synthesis of bis(alkylzinc)methoxide-bis(2-pyridylmethyl)amides

The reaction of **V** with water, even diluted as toluene solution, was reported to proceed quite violently and resulted in decomposition of the complex into numerous products [9]. In order to slow down the protonation reaction we treated amide **1** with one equivalent of methanol under kinetically controlled conditions (slow warming from −78 °C to r.t.). In the course of the reaction the μ-N(H)tBu moiety was substituted by a μ-OMe substituent quantitatively yielding complex **2**. As observed previously the Zn–C bond was not affected by the alcoholysis. Alternatively, bis(alkylzinc)methoxide-bis(2-pyridylmethyl)amides (**2**, **3**) were also accessible by zincation of stoichiometric amounts of methanol and dipicolylamine **II** with dialkylzinc at low temperatures (Fig. 6)

A comparison of the molecular structures of **2** and **3** shows very similar Zn1–N1 and Zn1–N2 bond lengths (Table 1) which are slightly shorter than in **1**. This observation is a result of the reduced steric demand of the μ-OMe moiety also being expressed by a nearly planar Zn$_2$NO ring. The Zn–C bond in **3** is slightly longer due to the bulkiness of the CH(SiMe$_3$)$_2$ substituents at the metal atoms. A slight (but not significant) difference with respect to the Zn–OMe bond is observed in **3** in comparison to **2**, being in agree-
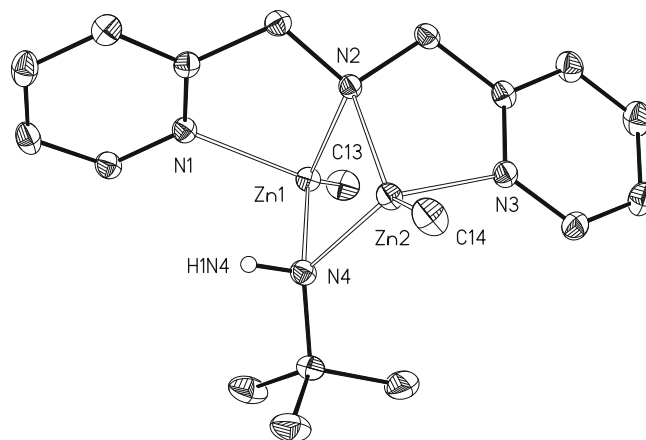

Fig. 5. Molecular structure and numbering of **1**. The hydrogen atoms with exception of the amido group are omitted for clarity. The ellipsoids of all non-hydrogen atoms represent a probability of 40%. Selected structural data can be found in Table 1.

ment with the Zn–O bond lengths found in [EtZn(py)(μ-O^{t}Bu)]$_2$ (198.8 pm) [18] and [EtZn(py)(μ-OCH(CF$_3$)$_2$)]$_2$ (210.4 pm) [19]. Alkylzinc alkoxides have recently gained interest as excellent precursors for the preparation of ceramic materials, nano particles and ZnO films (MOCVD) with semiconducting properties [18–20] (see Fig. 7).

An interesting feature is the differing geometry around O1 in the methoxides **2** and **3**. In **2** a planar environment is observed enabling a strong out of the plane oscillation of O1. In **3** a pyramidal geometry is realized which is caused by steric repulsion between the methoxy substituent and the bis(trimethylsilyl)methyl groups. The transannular Zn1···Zn2 contact is very similar in both complexes but slightly longer than in the folded ring structure of **1**.

2.3. NMR-investigations on **1**, **2** and **3**

In the ^{1}H NMR spectra (C$_6$D$_6$) of **1**, **2** and **3** the pyridyl resonances are very much alike. The major difference is observed for the Pyr 1 signal in **1** which splits up in two separate resonances due to the neighboring N4 carrying different substituents. For the very same reason the proton resonances of the methylene groups in **1** give two anisochronic signals. The Pyr 1 resonance in **3** is slightly shifted downfield compared to the corresponding signal of **2**. The ^{1}H NMR spectra of the latter shows very broad signals, possibly indicating the dismutation of the complex into different aggregates of [(MeZnOMe)$_n$] and dimeric **V**. A detailed theoretical investigation on the oligomerisation process of [MeZnOMe] monomers was given by Steudel et al. [21]. In the ^{13}C NMR spectrum a slight difference is only observed for the zinc bound methyl groups in **1** and **2** which are shifted upfield (3.5 ppm) when changing to Zn–O coordination.
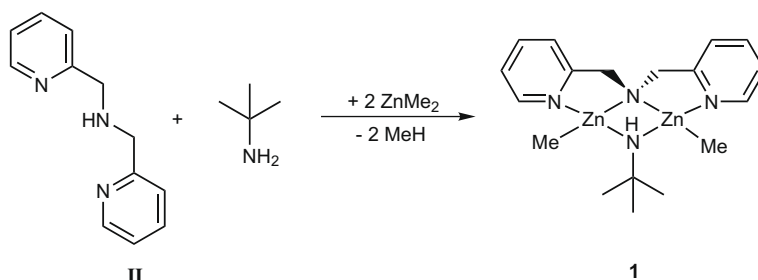

Fig. 4. Synthesis of bis(methylzinc)*t*-butylamide-bis(2-pyridylmethyl)amide **1**.
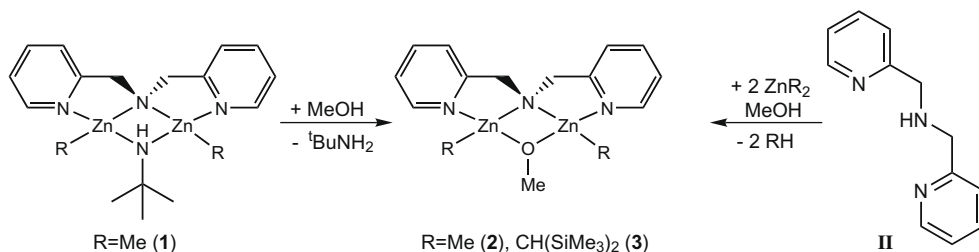
Fig. 6. Synthesis of bis(alkylzinc)methoxide-bis(2-pyridylmethyl)amides (**2**/**3**).

2.4. Reactivity of **1** and **2**

In order to evaluate the stability and reactivity of **1** towards other bases containing acidic hydrogen atoms the heteroleptic dimethylzinc amide **1** was exposed to an excess of phenylamine (aniline). Immediate cooling upon addition of the amine led to the deposition of a few crystals suitable for X-ray analysis. Quite surprisingly the expected exchange of the *t*-butylamide moiety in **1** against an anilide similar to the methanolysis reaction proceeded further under partial decomposition of the starting material (Fig. 8)

yielding the amide complex **4**. Since the obtained crystals were coated with dipicolylamine **II** a reliable determination of yield and melting point was impossible. Mechanistically we still assume an exchange of the bridging moiety as the initial reaction step. Subsequent insertion of a second equivalent of phenylamine leads to intermediate **I4** which features a $Zn[\mu-(N\cdots H\cdots N)]Zn$ functionality. The increased acidic nature of the bridging proton now enables the partial protonation of Zn–C as well as Zn–N2 bonds.

The centrosymmetric structure of **4** is assembled of two six-membered $[\{Zn(\mu-N(H)Ph)\}\{MeZn(\mu-N(H)Ph)\}_2\{\mu-N(CH_2Py)_2\}]$ rings which are interconnected via a central four-membered $Zn_2(\mu-N(H)Ph)_2$ unit. The ring expansion with the additional phenylamide has no effect on the Zn–C bond lengths compared to **2** and **3** whereas the Zn1/2–N2 bonds experience a slight shortening. The Zn1–N5 and Zn2–N6 bonds are almost identical and very similar to the average Zn–N bond length observed in dimeric $[MeZn(NPh_2)]_2$ (207.2(8) pm) [22]. Although being in a tetrahedral coordination sphere the Zn3–N5/N6 bond lengths are significantly shortened compared to $[MeZn(NPh_2)]_2$ arising from the increased ionic nature of Zn3. Within the $Zn_2(\mu-NHPh)_2$ ring the Zn–N bond lengths resemble those in $[MeZn(NPh_2)]_2$ [22].

The methoxide **2** readily dissolves in *t*-butylamine. Expecting the formation and eventually the crystallization of the intermediate **M-I** (Fig. 10) the solution was stored at 5 °C. After a period of two weeks colorless crystals precipitated which could be characterized by X-ray diffraction. To our surprise a trinuclear disiloxide complex $[(MeZn)_2\{\mu-N(CH_2Py)_2\}_2Zn\{\mu-(OMe_2Si)_2O\}]$ (**5**) was formed as a result of the accidental contact of the solution with silicone grease (Wacker) sealed ground glass joints. The ^{1}H NMR spectra of the mixture shows several singlet signals in the range 0.1–0.4 ppm indicating the presence of various types of silicone grease cleavage products. As demonstrated by Chang et al. the base

Table 1
Selected bond lengths (pm) and angles (°) of **1**, **2** and **3**.

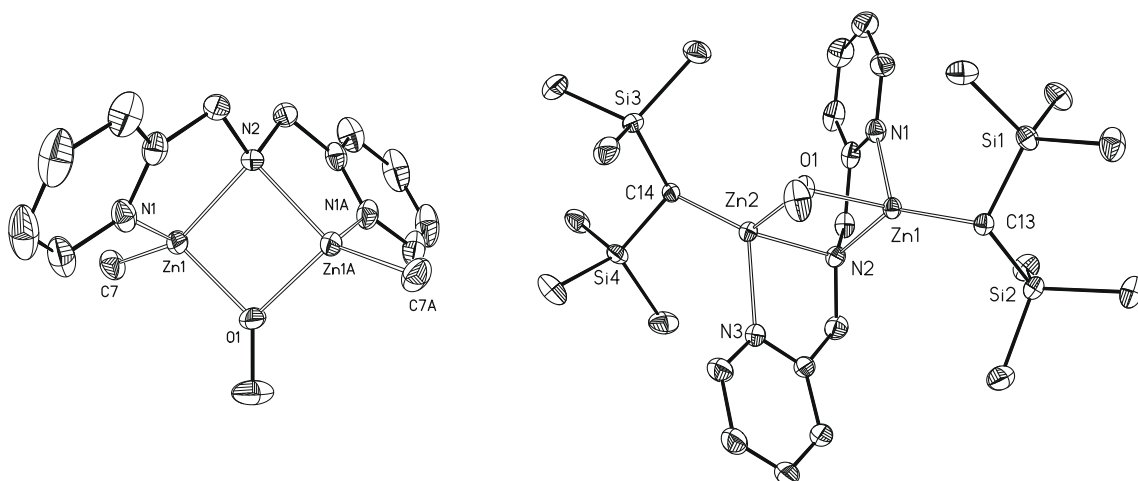|	**1**	**2**	**3**
Zn1–N1	216.3(2)	213.0(3)	215.1(3)
Zn1–N2	209.9(2)	206.8(2)	205.8(3)
Zn1–N4/O1	204.7(2)	197.7(2)	200.4(2)
Zn1–C$_{Zn}$	197.5(3)	197.0(3)	200.7(3)
Zn2–N2	208.8(2)	206.7(3)	
Zn2–N3	219.0(2)		211.9(3)
Zn2–N4/O1	203.8(2)		199.9(2)
Zn2–C14	198.2(2)		200.3(2)
Zn1···Zn1A/Zn2	285.8(4)	292.3(5)	290.4(5)
Zn1–N2–Zn1A/Zn2	86.1(1)	89.9(1)	89.5(1)
N2–Zn1–N4/O1	88.8(1)	87.4(1)	88.7(1)
N1–Zn1–C$_{Zn}$	124.4(1)	116.7(1)	124.4(1)
N2–Zn2–N4/O1	89.3(1)		88.6(1)
N3–Zn2–C14	110.7(1)		125.4(1)
Zn1–N4/O1–Zn1A/Zn2	88.8(1)	95.3(1)	93.0(1)
Zn1–N4/O1–C$_O$	125.8(2)	132.3(1)	121.0(2)
Zn2–N4/O1–C$_O$	126.1(2)		126.5(2)
C15–N4–H(1N4)	106(2)		

Fig. 7. Molecular structures and numbering schemes of **2** (to the left) and **3** (to the right). The hydrogen atoms are omitted for clarity. The ellipsoids represent a probability of 40%. Selected structural data can be found in Table 1.
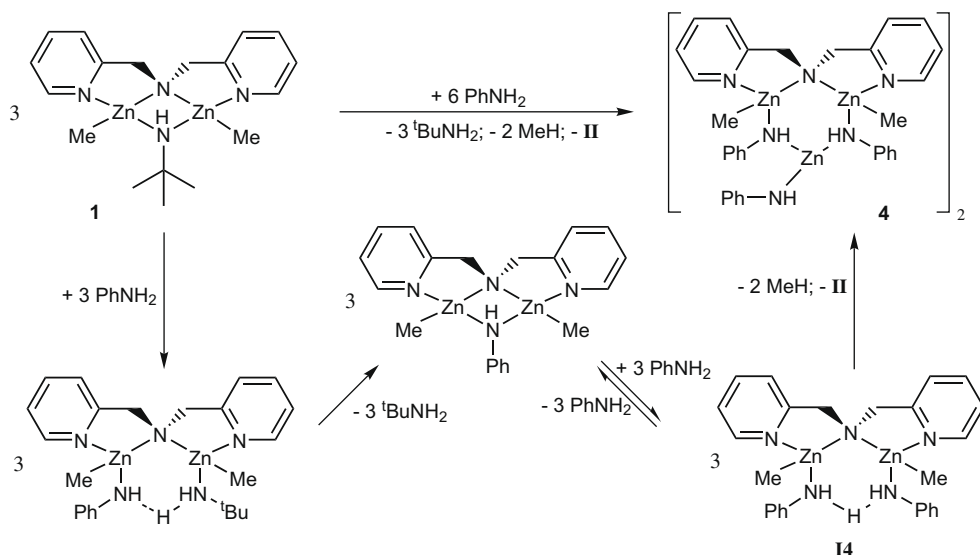
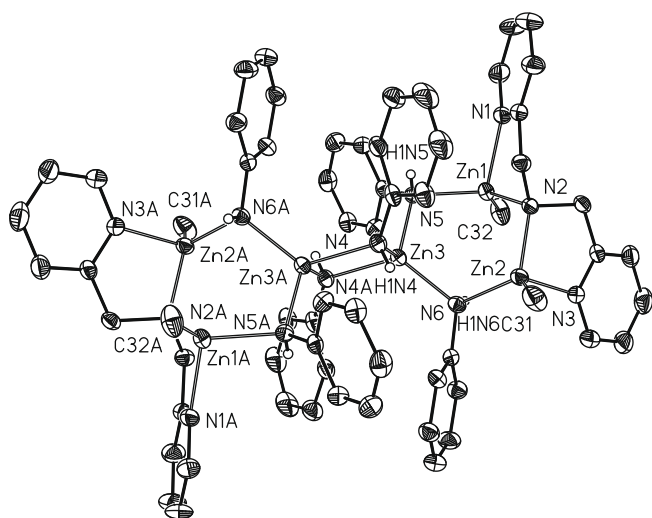Fig. 8. Aminolysis of 1 with aniline and subsequent degradation to 4.

Fig. 9. Molecular structure and numbering scheme of 4. The hydrogen atoms with exception of the anilide groups are omitted for clarity. The ellipsoids of all non-hydrogen atoms represent a probability of 40%. Symmetry related atoms ($-x + 1$, y, $-z$) are marked with an "A". Selected bond lengths (pm): Zn1–N1 218.6(3), Zn1–N2 204.9(2), Zn1–N5 208.4(3), Zn1–C32 197.5(3), Zn2–N2 204.4(2), Zn2–N3 213.0(3), Zn2–N6 208.4(3), Zn2–C31 198.0(3), Zn3–N4 205.3(2), Zn3–N5 202.2(3), Zn3–N6 201.5(3), Zn3–N4A 207.7(2).

catalyzed aminolysis of poly(dimethylsiloxane) is a feasible route leading to various oligo(dimethylsiloxan)amines and oligo(dimetylsiloxan)ols which may recondense in several side reactions [23]. The formation of such polysiloxane cleavage products is rather wide spread in the chemistry of highly polar organometallic reagents, the anion $O(SiMe_2O^-)_2$ being the most common one [24] (see Fig. 9).

The structure of complex 5 is a rare synthetic example for having zinc ions in a tetrahedral and octahedral coordination sphere within the same compound (Fig. 11). The basic dimeric skeleton is comprised of two four-membered Zn_2NO rings fused together with the octahedral zinc ion as sharing corner. The zinc ions are almost aligned on an axis (Zn1–Zn2–Zn3 angle 170.4°) with an identical non-bonding contact of 302.3(5) pm to each other. The bond lengths associated with Zn1 and Zn3 are very similar and in agreement to those discussed for the complex 2. Due to the expanded
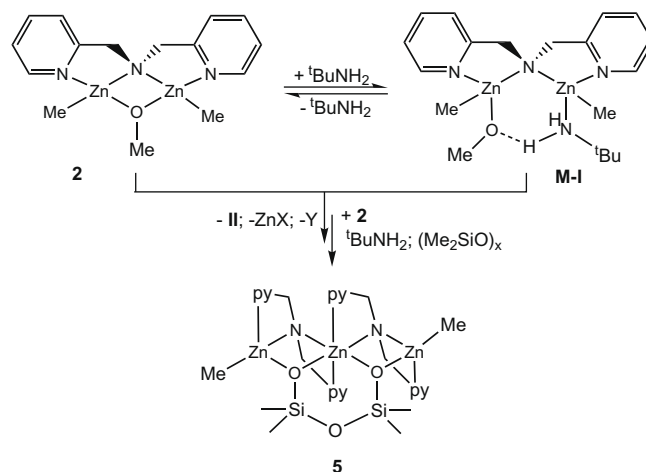

Fig. 10. Reaction of 1 with *t*-butylamine in the presence of adventitious silicone grease.

coordination sphere of Zn2 the Zn2–O1/Zn2–O2 bond lengths are noticeably larger (210.3(2)/215.9(2) pm) when compared to the Zn1–O1/Zn3–O3 bond lengths (199.9(2)/199.2(2) pm). A similar lengthening is observed for the Zn2–N2/Zn2–N5 bonds (221.7(3)/218.2(3) pm) whereas the Zn2–N3/Zn2–N4 bond distances (218.3(3)/217.3(3) pm) are quite comparable to the Zn1–N1 bond length in 1 (216.3(2) pm).

3. Mechanism of the methanolysis and aminolysis

3.1. Methanolysis of 1

When treating 1 with methanol one would expect the elimination of methane on the basis of pK_s values forming the corresponding methanolate, but instead an exchange of the μ-N(H)*t*Bu moiety is observed. Extensive DFT-calculations at the B3LYP/TZVP level of theory were carried out in order to reveal the underlying mechanism of this reaction, thus confirming and clarifying the experimental findings.

Considering the expected protonation of the zinc bound methyl group no stationary point on the hypersurface could be found
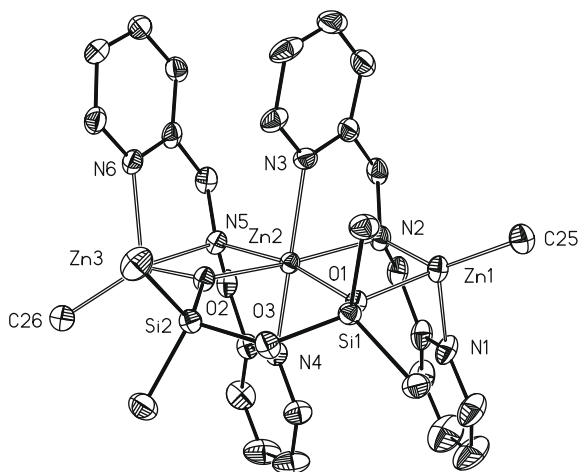
Fig. 11. Molecular structure and numbering scheme of **5**. The hydrogen atoms are omitted for clarity. The ellipsoids represent a probability of 40%. Selected bond lengths (pm): Zn1–N1 214.9(4), Zn1–N2 202.6(3), Zn1–O1 199.9(2), Zn1–C25 198.8(4), Zn2–O1 210.3(2), Zn2–O2 215.9(2), Zn2–N2 221.7(3), Zn2–N5 218.2(3), Zn2–N3 218.3(3), Zn2–N4 217.3(3), Zn3–O2 199.2(2), Zn3–N5 203.9(3), Zn3–N6 214.6(3), Zn3–C26 198.4(3).

favoring this reaction pathway. Instead the methanol molecule approaches the Zn1–N4 bond from the sterically less hindered side. Thus the methanol first comes in contact with the pyridyl proton in ortho-position to the aromatic nitrogen, leading to complex **M-E1**. From this position methanol can attack the Zn1–N4 bond via the transition structure **M-TS1** (rate determining step; ΔG = +21.1 kcal/mol, see Table 3) in a [2+2] fashion leading to the intermediate **M-I**. The latter intermediate features a Zn[μ-(O$\cdots$H$\cdots$N)]Zn functionality, having the bridging proton already closely bound to the amide. Then the oxygen atom in this three center bond attacks the zinc atom to generate a μ-OMe group. The former amino nitrogen is protonated in this step (**M-TS2**, ΔG = +5.6 kcal/mol) by the hydrogen atom originating from the methanol molecule. Complex **M-E2** is then formed before the t-butylamine molecule finally departs, yielding compound **2** (see Fig. 12).

To assess the robustness of the obtained energies, single point energy calculations on the optimized structures were carried out, using the double hybrid B2GP-PLYP functional, which has been claimed to deliver highly accurate thermochemistry values [25]. The parameters summerized in Table 3 support that the B2GP-

PLYP predictions are in good agreement with deviations of less than 3 kcal/mol to those obtained by the B3LYP functional.

3.2. Aminolysis of **1**

The synthesis of complex **2** through the conversion of **1** with methanol proceeds very fast even at low temperature. Thus, it is neither possible to find any spectroscopic evidence for the existence of the proposed pathway nor the corresponding intermediates. In order to follow up the calculated mechanism, compound **1** was reacted with an excess of t-butylamine (Fig. 13). This procedure resulted in an exchange process of the t-butylamide moiety involving the proposed intermediates (**Iza/b**). In this case z indicates an integer ($z = 1 - 3$) standing for the three different pathways which lead to different stereo isomers.

Considering a comparable mechanism to the methanolysis, the mechanism of the reaction path of **1** with t-butylamine follows similar steps (see Fig. 14). Approaching the binuclear complex **1** the amine first comes in contact with either the proton in ortho position of the pyridine ring (**Eza**) or the proton of the bridging amide (**Ezb**), leading to the formation of a complex via a loose hydrogen bond. From this position the insertion into one of the N4–Zn bonds is enabled over **TSza** and **TSzb**, respectively (rate determining step; $\Delta G \sim 30$ kcal/mol at B3LYP/TZVP level of theory, see Table 4). As a result, the intermediate structure (**Iza**; **Izb**) is generated, featuring a Zn[μ-(N$\cdots$H$\cdots$N)]Zn functionality. With a barrier of ca. 4 kcal/mol (cf. Table 4) the bridging proton is able to migrate easily between the two amino groups (**TSIzab**). The amine escapes from the six membered ring similar to the way of insertion, yielding **1**.

The exchange progress can be followed by ^{1}H NMR spectroscopy. The ^{1}H NMR spectra of **1** shows two different signals for the py1 protons (8.22 ppm, 8.01 ppm, see Table 2) due to the neighboring N4 atom which breaks the C2-symmetry of the molecule. When additional t-butylamine is added the magnetically in-equivalent py1/1′ signals merge to give one doublet with an averaged shift at 8.10 ppm. This can be understood in terms of an exchange of the t-butylamide which is fast on the NMR time scale. Temperature-dependent NMR studies show that the chemical shift is temperature-dependent and that the signal splits into two resonances at low temperatures as shown in Fig. 15. Furthermore, three additional doublet resonances appear at 8.17, 8.23 and 8.31 ppm.

Consisting of two stereo centers the number of possible stereo isomers of the intermediate structures **Iza/b** is, according to 2^n (with n = number of stereo centers), equal to four. Those include two enantiomers (**I2a**; **I2b**), which can be easily converted into each other via proton transfer (**TSI2ab**), and two diastereomers (**I1a**; **I3a**), all shown in Fig. 16. Proton transfer in the latter via the transition structures **TSI1ab** and **TSI3ab** leads to the intermediate structures **I1b** and **I3b** which are identical to **I1a** and **I3a**, respectively.

Table 3
Gibb's free energies of the methanolysis reaction, calculated at the B3LYP/TZVP and the B2GP-PLYP/cc-PVTZ level of theory. The values are given relative to **1** and a free methanol molecule.

	B3LYP/TZVP	B2GP-PLYP/cc-pVTZ
1 + MeOH	0.0	0.0
M-E1	13.1	13.4
M-TS1	21.4	24.5
M-I	0.1	2.1
M-TS2	5.6	7.5
M-E2	−6.3	−6.4
2 + ^{t}BuNH$_2$	−16.7	−16.7

Table 2
NMR chemical shifts (ppm) at 30 °C for the compounds **1**, **2** and **3**.

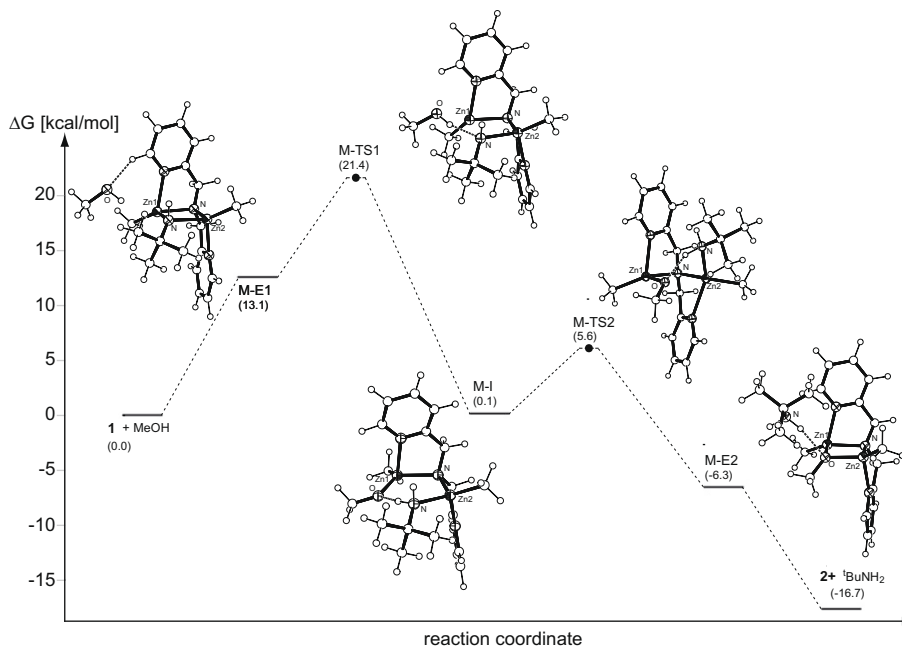| δ	**1**	**2**	**3**
^{1}H			
Pyr 1	8.22/8.01	8.04	8.22
Pyr 4	6.66	6.63	6.73
Pyr 3	6.88	6.84	6.91
Pyr 2	6.47	6.39	6.53
CH$_2$N	4.28/4.21	4.07	4.24
ZnMe	−0.40	−0.41	−1.24
OMe	–	3.93	3.79
^{13}C			
Pyr 1	147.4/146.7	147.4	147.5
Pyr 2	122.4	122.1	122.9
Pyr 3	137.4	137.6	138.1
Pyr 4	122.0	121.1	122.7
Pyr 5	163.1/162.9	161.7	160.8
CH$_2$N	61.4/61.3	60.3	59.7
ZnMe/ZnCH	−15.2	−18.8	−3.0
OMe/(NCtBu)	(51.0)	54.6	55.2

Fig. 12. Energy diagram of the methanolysis pathway of compound **1**, calculated at the B3LYP/TZVP level of theory. The values are given in kcal/mol relative to **1** and a free methanol molecule. The optimized structures can be found in the Supplementary Material in Fig. S1.
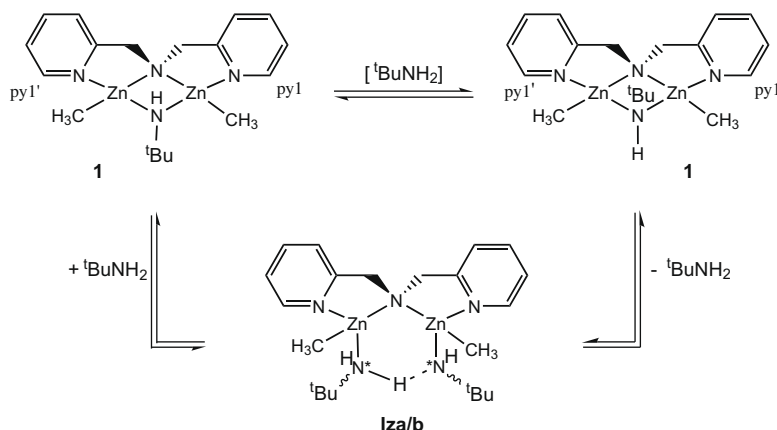

Fig. 13. Reaction of **1** with *t*-butylamine.

The nuclear magnetic shielding constants of the intermediates (**Iza/b**) and the involved transition structures (**TSIzab**) were calculated at the B3LYP/6-31++G(d,p) level of theory. Calibrating the average magnetic shielding constant of the py1/1′ protons in **I2a** on the experimental value of 8.23 ppm gives the chemical shifts for the other structures which are listed in Table 5. Due to the proton behavior only the average chemical shift of each triple (**Iza** $\rightleftharpoons$ **TSIzab** $\rightleftharpoons$ **Izb**) was considered as observable value. As expected the two enantiomeric structures **I2a** and **I2b** show the same chemical shift predisposed to 8.23 ppm. The calculated chemical shift of the diastereomeric intermediates **I1a** (8.34 ppm) and **I3a** (8.11 ppm) differ by 0.23 ppm and are in very good agreement to the observed experimental values of 8.31 and 8.17 ppm, respectively.

Based on the calculated Gibb's free energy of the transition structures **TSza/b**, which are similar, presuming an error of 3 kcal/mol, each of the four intermediates **Iza/b** has the same chance to be formed if the reaction is kinetically controlled. Therefore the signal intensity ought to follow a ratio of **I1a:I2a/**

b:I3a = 1:2:1 and indeed the signal at 8.23 ppm which corresponds to **I2a** and **I2b** is the most prominent one. However, an exact match of the intensity ratio was not obtained.

Despite of the slight incongruence in the signal intensity ^{1}H NMR spectroscopy in combination with quantum chemical calculations delivers a reasonable evidence for the existence of Zn[μ-(X···H···Y)]Zn (X = O, N; Y = N) functionalities in the mechanism of alcoholysis and aminolyses of **1** and hence support the conclusions.

4. Conclusions

The DFT calculations propose a mechanism for the experimentally observed exchange of the N(H)*t*Bu moiety in **1** when protolyzed with methanol. The importance of the intermediate Zn[μ-(X···H···Y)]Zn (X = O/N, Y = N) functionalities could be verified. Furthermore their existence was supported by ^{1}H NMR
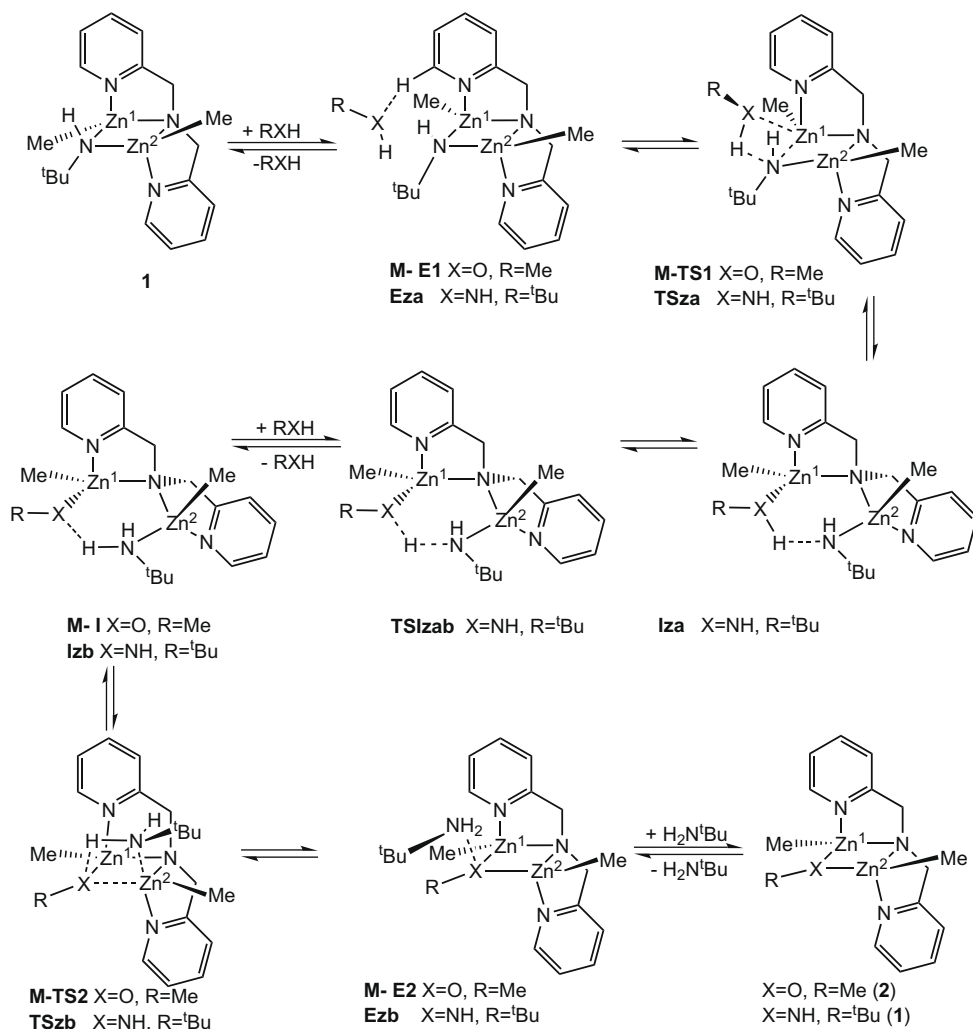
Fig. 14. Aminolysis and methanolysis pathway of compound **1**. The optimized structures, calculated at the B3LYP/TZVP level of theory, can be found in the supplementary material (Figs. S1–S4). The corresponding Gibb's free energies are summerized in Tables 3 and 4.

Table 4
Gibb's free energies of the aminolysis reaction, calculated at the B3LYP/TZVP level of theory. They are given relative to **1** and a free t-butylamine molecule. The three different pathways are indicated by the integer z (z = 1 − 3).

	ΔG (z = 1)	ΔG (z = 2)	ΔG (z = 3)
1 + tBuNH$_2$	0.0	0.0	0.0
Eza	7.2	7.8	8.9
TSza	29.6	31.6	29.4
Iza	14.5	14.5	14.6
TSIzab	18.7	20.6	18.0
Izb	14.5	16.3	14.6
TSzb	29.6	26.8	29.4
Ezb	7.2	10.2	8.9
1 + tBuNH$_2$	0.0	0.0	0.0

spectroscopy. We are now exploring their use in catalysis in order to evaluate their catalytic activity and the value of these complexes as a biomimetic model for binuclear zinc hydrolases.

Fig. 15. D NMR studies of compound **1** (solvent: [D$_8$]toluene). Only the ^{1}H NMR spectra of the resonances of the pyridyl protons in ortho position to the nitrogen (py1; py1′) are shown.

5. Computational details

All geometry optimizations were performed with the gradient-corrected hybrid B3LYP [26] density functional using the quantum chemical program package Turbomole [27]. The TZVP basis set based on the w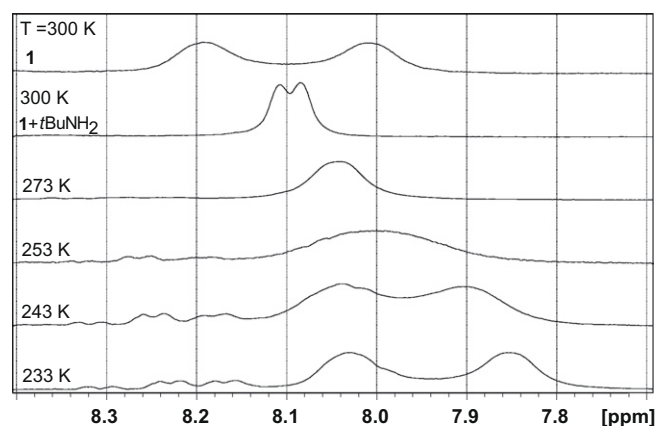ork of Schäfer et al. [28] was employed for the first row atoms as implemented in Turbomole. For the zinc ions a Stuttgart relativistic pseudopotential (known as ECP 10 MDF) has been employed [29]. All species found on the hypersurface were charac-
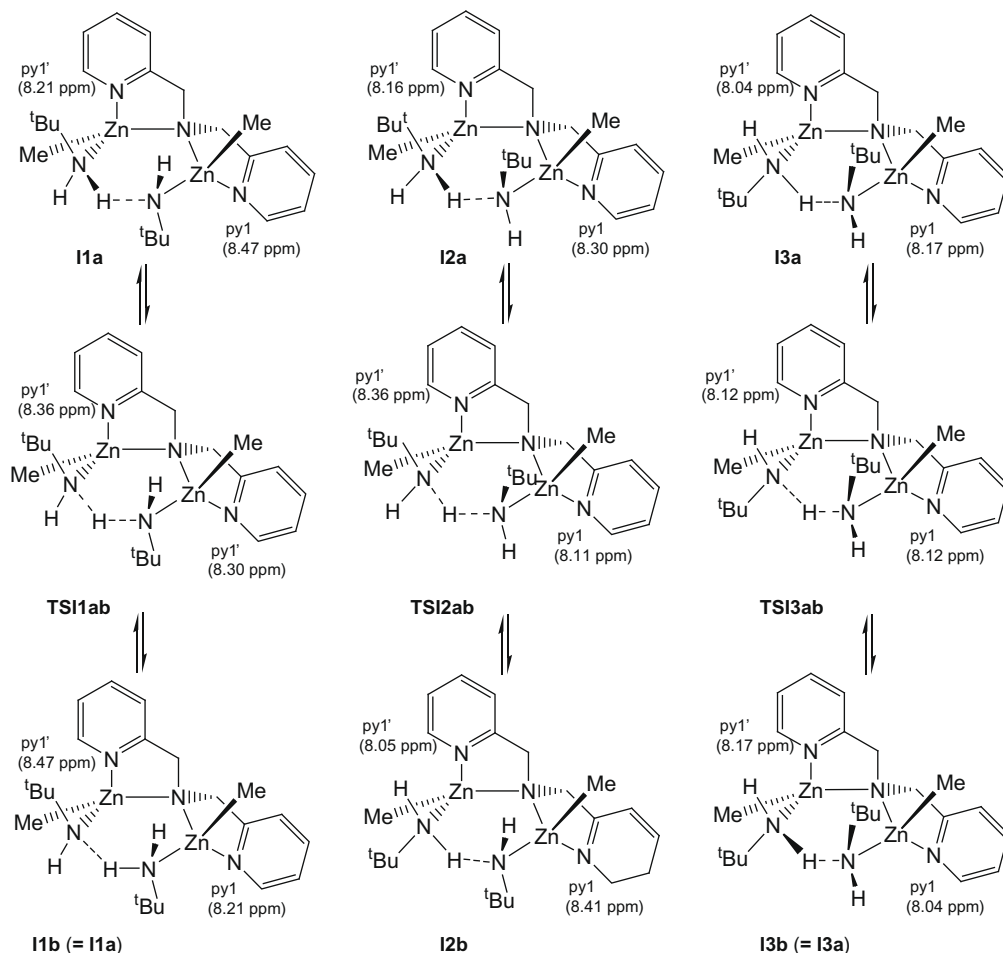
Fig. 16. Stereoisomeric intermediates created by the reaction of **1** with *t*BuNH₂.

Table 5
Calculated and experimental chemical shifts [ppm] for **1**, **Iza/b** and **TSIzab**.

	Calc. Chem. Shift [ppm]				Exp. Chem. Shift [ppm]	
	py1′	py1		Average	py1′	py1
1	7.99	8.20	8.11		8.01	8.22
I1a	8.21	8.47	8.34			
TSI1ab	8.36	8.30	8.33	**8.34**	8.31	
I1b	8.47	8.21	8.34			
I2a	8.16	8.30	8.23			
TSI2ab	8.36	8.11	8.24	**8.23**	8.23	
I2b	8.05	8.41	8.23			
I3a	8.04	8.17	8.11			
TSI3ab	8.12	8.12	8.12	**8.11**	8.17	
I3b	8.17	8.04	8.11			

terized as energetic minima or transition structures via vibrational analyses. Default convergence criteria were used and no symmetry was employed in all the calculations. The relative stabilities are reported as gas phase Gibbs free energies containing standard thermochemical (298 K) and vibrational corrections. In order to obtain more reliable energy data we have carried out single-point energy calculations on the B3LYP/TZVP optimized geometries with the GAUSSIAN03 [30] program package using the double hybrid B2GP-PLYP functional which was implemented as described [25]. The correlation consistent cc-pVTZ [31] basis set was applied to the C, N, O and H atoms and the Stuttgart pseudopotential (ECP 10 MDF) to the zinc ions [29]. The calculation of the magnetic shield-

ing constants was performed with the hybrid B3LYP functional using the 6-31++G(d,p) basis as implemented in the GAUSSIAN program package [30].

6. Experimental

6.1. General remarks

All reactions were performed in an argon atmosphere using standard Schlenk techniques. All solvents were dried and thoroughly deoxygenated according to standard procedures prior to use. IR spectra were recorded using Nujol suspensions between KBr windows. The starting material Zn[CH(SiMe₃)₂]₂ was prepared by a known procedure [32].

6.2. Synthesis of [(MeZn)₂{μ-N(H)t Bu}{μ-N(CH₂Py)₂}] (**1**)

A mixture of bis(2-pyridylmethyl)amine (**II**) (0.60 g, 3.0 mmol) and *t*-butylamine (0.22 g, 3.0 mmol) was dissolved in 10 ml of toluene and cooled to −78 °C. To the stirred solution 5.0 ml (6.0 mmol) of a 1.2 M solution of dimethylzinc in toluene were added dropwise. The reaction mixture turned claret red whilst methane was slowly liberated. After being warmed to r.t. the solution was stirred for additional 14 h. The volume of the solution was reduced to a few milliliters. Cooling of this solution to 5 °C led to the precipitation of colorless crystals of **1**. Yield 1.02 g (79%). M.p.: 85 °C (decomposition). NMR (C₆D₆, 300 K): ¹H: δ = 8.22 (s (br), 1 H, Pyr1); 8.01 (s (br), 1H, Pyr1′); 6.88 (dt, ³*J*(*H*,*H*) = 7.6 Hz,

$^4J(H,H)$ = 1.6 Hz, 2H, Pyr3/3′), 6.66 (d, $^3J(H,H)$ = 7.6 Hz, 2H, Pyr4/4′); 6.47 (m, 2H, Pyr2/2′); 4.28 (s, 2H, CH₂N); 4.21 (s, 2H, CH′₂N); 1.28 (s, 9H, C(CH₃)₃); 0.00 (s, 1H, NH), and −0.40 (s, 6H, ZnCH₃). $^{13}C\{^1H\}$: δ = 163.1 (Pyr5); 162.9 (Pyr5′); 147.4 (Pyr1); 146.7 (Pyr1′); 137.4 (Pyr3/3′), 122.4 (Pyr2/2′), 122.0 (Pyr4/4′), 61.4 (CH₂N), 61.3 (CH′₂N), 51.0 (C(CH₃)₃), 35.2 (C(CH₃)₃), and −15.2 (ZnCH₃). IR (cm⁻¹): 3271 w, 2925 vs, 2854 vs, 2761 m, 1990 w, 1913 w, 1841 w, 1645 m, 1602 s, 1568 s, 1462 vs, 1378 s, 1365 s, 1343 s, 1283 s, 1220 s, 1150 s, 1099 m, 1045 s, 1015 m, 959 m, 888 w, 812 w, 757 s, 729 s, 637 s, 560 m, 503 s. MS (EI, m/z) 413 ([M(⁶⁴Zn/⁶⁴Zn)−CH₃]⁺, 0.4%); 262 ([C₁₂H₁₂N₃⁶⁴Zn]⁺, 1.7%); 198 ([C₈H₁₀N₂⁶⁴Zn]⁺, 1.2%); 107 ([C₆H₇N₂]⁺, 21%); 93 ([C₆H₇N]⁺, 61%); 58 ([C₃H₈N]⁺, 100%). Anal. Calc. for C₁₈H₂₈N₄Zn₂ (431.18 g/mol): C, 50.13; H, 6.54; N, 12.99. Found: C, 49.44; H, 6.38; N, 13.00%.

6.3. Synthesis of [(MeZn)₂(μ-OMe){μ-N(CH₂Py)₂}] (2)

6.3.1. Procedure A

Bis(methylzinc)t-butylamide-bis(2-pyridylmethyl)amide (1) (0.30 g, 0.7 mmol) was dissolved in 7 ml of toluene and cooled to −78 °C. Then 0.7 ml of a 1.0 M solution of methanol in toluene (0.7 mmol) were added. The reaction mixture was slowly warmed to r.t. and afterwards concentrated under vacuum. At 5 °C colorless crystals of 2 precipitated. Yield 0.25 g (90%).

6.3.2. Procedure B

A mixture of bis(2-pyridylmethyl)amine (II) (0.60 g, 3.0 mmol) and 3.0 ml of a 1.0 M solution of methanol in toluene (3.0 mmol) was dissolved in 15 ml of toluene and cooled to −78 °C. To the stirred solution 5.0 ml of a 1.2 M solution of dimethylzinc in toluene (6.0 mmol) were added dropwise. The mixture was slowly warmed to r.t. and concentrated under vacuo thereafter. Cooling of this solution to 5 °C afforded the precipitation of colorless crystals of 2. Yield 0.96 g (82%). M.p.: 127 °C. NMR (C₆D₆, 300 K): ^1H: δ = 8.04 (s (br), 2H, Pyr1); 6.84 (m, 2H, Pyr3); 6.63 (s (br), 2H, Pyr4); 6.39 (m, 2H, Pyr2); 4.07 (s, 4H, CH₂N); 3.93 (s, 3H, OCH₃); −0.41 (s, 6H, ZnCH₃). $^{13}C\{^1H\}$: δ = 161.7 (Pyr5); 147.4 (Pyr1); 137.6 (Pyr3); 122.1 (Pyr2/4); 60.3 (CH₂N); 54.6 (OCH₃); −18.8

(ZnCH₃). IR (cm⁻¹): 2925 vs, 2854 vs, 2763 m, 2266 w, 2169 w, 1999 w, 1957 w, 1912 w, 1845 w, 1779 w, 1720 w, 1651 m, 1603 s, 1569 s, 1464 vs, 1379 s, 1343 s, 1285 s, 1235 s, 1213 m, 1150 s, 1096 s, 1048 s, 980 m, 957 m, 893 w, 811 m, 757 s, 728 s, 639 vs, 520 s. MS (EI, m/z): 372 ([M(⁶⁴Zn/⁶⁴Zn)−CH₃]⁺, 2.2%); 342 ([C₁₂H₁₂N₃O⁶⁴Zn₂]⁺, 0.9%); 262 ([C₁₂H₁₂N₃⁶⁴Zn]⁺, 4.6%); 200 ([C₁₂H₁₄N₃]⁺, 6.9%) 198 ([C₈H₁₀N₂⁶⁴Zn]⁺, 3.2%); 107 ([C₆H₇N₂]⁺, 87%); 93 ([C₆H₇N]⁺, 100%). Anal. Calc. for C₁₅H₂₁N₃Zn₂ (390.13 g/mol): C, 46.18; H, 5.43; N, 10.77. Found: C, 45.33; H, 5.51; N, 10.67%.

6.4. Synthesis of [{(Me₃Si)₂CHZn}₂(μ-OMe){μ- N(CH₂Py)₂}] (3)

A mixture of bis(2-pyridylmethyl)amine (II) (0.60 g, 3.0 mmol) and 3.0 ml of a 1.0 M solution of methanol in toluene (3.0 mmol) was dissolved in 3 ml of toluene and cooled to −78 °C. To the stirred solution 12.0 ml of a 0.5 M of bis[bis(trimethyl-silyl)methyl]zinc in toluene (6.0 mmol) were added dropwise. After being warmed to r.t. the solution was stirred for additional 14 h. The volume of the solution was reduced to a few milliliters. Cooling of this solution to 5 °C led to the precipitation of colorless crystals of 3. Yield 1.60 g (78%). M.p.: 98 °C. NMR (C₆D₆, 300 K): ^1H: δ = 8.22 (d, $^3J(H,H)$ = 4.8 Hz, 2H, Pyr1); 6.91 (dt $^3J(H,H)$ = 7.6 Hz, $^4J(H,H)$ = 1.6 Hz, 2H, Pyr3); 6.73 (d, $^3J(H,H)$ = 7.6 Hz, 2H, Pyr4); 6.53 (m, 2H, Pyr2); 4.24 (s, 4H, CH₂N); 3.79 (s, 3H, OCH₃); 0.13 (s, 36H, CH(Si(CH₃)₃)₂); −1.24 (s, 2H, ZnCH(SiMe₃)₂). $^{13}C\{^1H\}$: δ = 160.8 (Pyr5); 147.5 (Pyr1); 138.1 (Pyr3); 122.9 (Pyr4); 122.7 (Pyr2); 59.7 (CH₂N); 55.2 (OCH₃); 4.7 (CH(Si(CH₃)₃)₂); −3.0 (ZnCH(SiMe₃)₂). IR (cm⁻¹): 2924 vs, 2854 vs, 2742 m, 2677 w, 1984 w, 1950 w, 1912 w, 1840 w, 1640 w, 1606 s, 1571 m, 1456 vs, 1377 s, 1343 m, 1285 m, 1240 s, 1153 m, 1125 m, 1101 m, 1077 m, 1045 s, 1021 s, 980 m, 852 vs, 830 vs, 771 s, 755 s, 668 s, 642 m, 607 m, 488 s. MS (EI, m/z): 660 ([M(⁶⁴Zn/⁶⁴Zn)−CH₃]⁺, 22%); 645 ([M(⁶⁴Zn/⁶⁴Zn)−2CH₃]⁺, 20%); 520 ([M(⁶⁴Zn/⁶⁸Zn)−CH(SiMe₃)₂]⁺, [M(⁶⁶Zn/⁶⁶Zn)−CH(SiMe₃)₂]⁺, 100%); 262 ([C₁₂H₁₂N₃⁶⁴Zn]⁺, 85%); 198 ([C₁₂H₁₂N₃]⁺, 73%). Anal. Calc. for C₂₇H₅₃N₃OSi₄Zn₂ (678.85 g/mol): C, 47.77; H, 7.87; N, 6.19. Found: C, 48.07; H, 7.94; N, 5.85%.

Table 6
Crystal data and refinement details for the X-ray structure determination.

Compound	1	2	3	4	5
Formula	C₁₈H₂₈N₄Zn₂	C₁₅H₂₁N₃OZn₂	C₂₇H₅₃N₃OSi₄Zn₂	C₆₄H₇₂N₁₂Zn₆ · 2 C₇H₈	C₃₀H₄₂N₆O₃Si₂Zn₃
Fw (g · mol⁻¹)	431.18	390.09	678.82	1585.82	786.99
T (°C)	−90(2)	−90(2)	−90(2)	−90(2)	−90(2)
Crystal system	Triclinic	Monoclinic	Monoclinic	Triclinic	Triclinic
Spacegroup	P1̄	C2/c	P2₁/n	P1̄	P1̄
a (Å)	8.9787(4)	16.1318(7)	17.1250(6)	11.9392(5)	10.4652(5)
b (Å)	9.5358(4)	11.1350(5)	10.3814(2)	13.3651(8)	10.9809(7)
c (Å)	12.3484(6)	9.5169(3)	21.0288(9)	13.4461(7)	15.7968(6)
α (°)	86.494(2)	90	90	117.482(2)	99.717(3)
β (°)	82.775(2)	101.420(3)	104.135(2)	94.431(3)	94.430(3)
γ (°)	74.631(2)	90	90	93.689(3)	95.046(3)
V (Å³)	1010.93(8)	1675.65(12)	3625.3(2)	1885.60(17)	1774.49(16)
Z	2	4	4	1	2
ρ (g · cm⁻³)	1.417	1.546	1.244	1.397	1.473
μ (cm⁻¹)	23.79	28.64	14.78	19.28	21.17
Measured data	7241	5734	24921	13367	12613
Measured data (I > 2σ(I))	3777	1597	5563	6188	4967
Unique data (R_int)	4580/0.0270	1907/0.0690	8256/0.0718	8473/0.0284	8089/0.0396
wR₂ (all data, on F²)ᵃ	0.0887	0.0985	0.1085	0.0999	0.1059
R₁ (I > 2σ(I))ᵃ	0.0330	0.0377	0.0457	0.0417	0.0457
sᵇ	1.009	1.022	0.998	1.007	0.957
Residual density (eÅ⁻³)	0.612/−0.610	0.169/0.623/−0.741	0.641/−0.455	0.523/−0.466	0.477/−0.632
CCDC no.	740264	740265	740266	740267	740268

ᵃ Definition of the R indices: $R_1 = (\sum ||F_o| - |F_c||) / \sum |F_o|$. $wR_2 = \sqrt{\sum [w(F_o^2 - F_c^2)^2] / \sum [w(F_o^2)^2]}$ with $w^{-1} = \sigma^2(F_o^2) + (aP)^2$.

ᵇ $s = \sqrt{\sum [w(F_o^2 - F_c^2)^2] / (N_o - N_p)}$.

6.5. Synthesis of [{Zn(μ-N(H)Ph)}{MeZn(μ-N(H)Ph)}$_2${μ- N(CH$_2$Py)$_2$}]$_2$ (**4**)

Phenylamine (aniline, 0.23 ml, 2.5 mmol) was added dropwise to a solution of bis(methylzinc)t-butylamide-bis(2-pyridyl-methyl)-amide (**1**) (0.27 g, 0.63 mmol) in 5 ml toluene. The light red solution was stirred for 1 h whereupon the volume was reduced to 1 ml. Cooling of this solution to 5 °C led to the precipitation of colorless crystals of **4**. Estimated yield: 20%. NMR (C$_6$D$_6$, 300 K): ^{1}H: δ = 7.60 (s (br), 2H, Pyr1); 7.10–7.00 (m, Ph); 6.88 (m, Pyr3); 6.74–6.20 (m Ph/Pyr4); 6.39 (m, Pyr2); 4.17 (s, 4H, CH$_2$N); 2.84 (s (br), NH); −0.29 (s, 6H, ZnCH$_3$).

6.6. Crystal structure determinations

The intensity data for the compounds **1**-**5** were collected on a Nonius Kappa CCD diffractometer using graphite-monochromated Mo Kα radiation. Data were corrected for Lorentz and polarization effects but not for absorption effects [33,34]. Crystallographic data as well as structure solution and refinement details are summarized in Table 6. The structures were solved by direct methods (SHELXS [35]) and refined by full-matrix least squares techniques against Fo^2 (SHELXL-97 [36]). The hydrogen atoms were located by difference Fourier synthesis and refined isotropically for the methyl groups C13/C14 of compound **1** and **2** and for the amide groups at N4, N5 and N6 of compound **1** and **4**. The other hydrogen atoms were included at calculated positions with fixed thermal parameters. All non-hydrogen atoms were refined anisotropically [36]. XP (SIEMENS Analytical X-ray Instruments, Inc.) was used for structure representations.

Acknowledgements

Appendix A. Supplementary data

CCDC 740264,740265, 740266 and 740267 contains the supplementary crystallographic data for **1**, **2**, **3** and **4**. These data can be obtained free of charge from The Cambridge Crystallographic Data Centre via www.ccdc.cam.ac.uk/data_request/cif. Supplementary data associated with this article can be found, in the online version, at doi:10.1016/j.jorganchem.2009.09.041.

References

[1] (a) W.T. Lowther, B.W. Matthews, Chem. Rev. 102 (2002) 4581;
(b) N. Sträter, W.N. Lipscomb, T. Klabunde, B. Krebs, Angew. Chem., Int. Ed. Engl. 35 (1996) 2024;
(c) W.N. Lipscomb, N. Sträter, Chem. Rev. 96 (1996) 2375;
(d) D.E. Wilcox, Chem. Rev. 96 (1996) 2435.
[2] J. Weston, Chem. Rev. 105 (2005) 2151.
[3] G. Parkin, Chem. Rev. 104 (2004) 699.
[4] H.-B. Kraatz, N. Metzler-Nolte, Concepts and Models in Bioinorganic Chemistry, Wiley-VCH, Weinheim, 2006.
[5] M. Westerhausen, T. Bollwein, P. Mayer, H. Piotrowski, A. Pfitzner, Z. Anorg. Allg. Chem. 628 (2002) 1425.
[6] M. Westerhausen, T. Bollwein, N. Makropoulos, T.M. Rotter, T. Habereder, M. Suter, H. Nöth, Eur. J. Inorg. Chem. (2001) 851.
[7] M. Westerhausen, T. Bollwein, N. Makropoulos, S. Schneiderbauer, M. Suter, H. Nöth, P. Mayer, H. Piotrowski, K. Polborn, A. Pfitzner, Eur. J. Inorg. Chem. (2002) 389.
[8] M. Westerhausen, A.N. Kneifel, I. Lindner, J. Grčić, H. Nöth, Z. Naturforsch. 59 (2004) 161.
[9] E. Jaime, A.N. Kneifel, M. Westerhausen, J. Weston, J. Organomet. Chem. 693 (2008) 1027.
[10] M. Westerhausen, A.N. Kneifel, Inorg. Chem. Comm. 7 (2004) 763.
[11] (a) P.C. Andrews, D.R. Armstrong, D.R. Baker, R.E. Mulvey, W. Clegg, L. Horsburgh, P.A. O'Neil, D. Reed, Organometallics 14 (1995) 427;
(b) P.C. Andrews, R.E. Mulvey, W. Clegg, D. Reed, J. Organomet. Chem. 386 (1990) 287;
(c) P.C. Andrews, D.R. Armstrong, R.E. Mulvey, D. Reed, J. Am. Chem. Soc. 110 (1988) 5235.
[12] (a) F. Meyer, Eur. J. Inorg. Chem. (2006) 3789;
(b) B. Bauer-Siebenlist, F. Meyer, E. Farkas, D. Vidovic, S. Dechert, Chem. Eur. J. 11 (2005) 4349;
(c) B. Bauer-Siebenlist, F. Meyer, E. Farkas, D. Vidovic, J.A. Cuesta-Seijo, R. Herbst-Irmer, H. Pritzkow, Inorg. Chem. 43 (2004) 4189;
(d) F. Meyer, P. Rutsch, Chem. Commun. (1998) 1037;
(e) M. Ruf, K. Weis, H. Vahrenkamp, J. Am. Chem. Soc. 118 (1996) 9288.
[13] N.V. Kaminskaia, C. He, S. Lippard, Inorg. Chem. 39 (2000) 3365.
[14] D. Suarez, E.N. Brothers, K.M. Merz Jr., Biochemistry 41 (2002) 6615.
[15] S. Erhardt, E. Jaime, J. Weston, J. Am. Chem. Soc. 127 (2005) 3654.
[16] M.M. Olmstead, W.J. Grigsby, D.R. Chacon, T. Hascall, P.P. Power, Inorg. Chim. Acta 251 (1996) 273.
[17] A. Almenningen, T.U. Helgaker, A. Haaland, S. Samdal, Acta Chem. Scand., Ser. A 36 (1982) 159.
[18] T.J. Boyle, S.D. Bunge, N.L. Andrews, L.E. Matzen, K. Sieg, M.A. Rodriguez, T.J. Headley, Chem. Mater. 16 (2004) 3279.
[19] S. Suh, L.A. Mîinea, S. Javed, D.M. Hoffman, Polyhedron 27 (2008) 513.
[20] C.D. Chandler, C. Roger, M.J. Hampden-Smith, Chem. Rev. 93 (1993) 1205.
[21] R. Steudel, Y. Steudel, J. Phys. Chem. A 110 (2006) 8912.
[22] N.A. Bell, H.M.M. Shearer, C.B. Spencer, Acta Cryst. C 39 (1983) 1182.
[23] C.L. Chang, H.S. Lee, C.K. Chen, J. Polym. Res. 12 (2005) 433;
C.L. Chang, Y.K. Lin, Polym. Degrad. Stab. 87 (2005) 207.
[24] I. Haiduc, Organometallics 23 (2004) 3.
[25] A. Karton, A. Tarnopolsky, J. Lamère, G.C. Schatz, J.M.L. Martin, J. Phys. Chem. A 112 (2008) 12868.
[26] (a) A.D. Becke, J. Chem. Phys. 98 (1993) 5648;
(b) C. Lee, W. Yang, R.G. Parr, Phys. Rev. B 37 (1988) 785.
[27] (a) F. Weigend, M. Häser, H. Patzelt, R. Ahlrichs, Chem. Phys. Lett. 294 (1998) 143;
(b) F. Haase, R. Ahlrichs, J. Comput. Chem. 14 (1993) 907;
(c) R. Ahlrichs, M. Bär, M. Häser, H. Horn, C. Kölmel, Chem. Phys. Lett. 162 (1989) 165;
(d) C. Møller, M.S. Plesset, Phys. Rev. 46 (1934) 618.
[28] A. Schäfer, C. Huber, R. Ahlrichs, J. Chem. Phys. 100 (1994) 5829.
[29] M. Dolg, U. Wedig, H. Stoll, H. Preuss, J. Chem. Phys. 86 (1987) 866.
[30] M.J. Frisch, G.W. Trucks, H.B. Schlegel, G.E. Scuseria, M.A. Robb, J.R. Cheeseman, J.A. Montgomery Jr., T. Vreven, K.N. Kudin, J.C. Burant, J.M. Millam, S.S. Iyengar, J. Tomasi, V. Barone, B. Mennucci, M. Cossi, G. Scalmani, N. Rega, G.A. Petersson, H. Nakatsuji, M. Hada, M. Ehara, K. Toyota, R. Fukuda, J. Hasegawa, M. Ishida, T. Nakajima, Y. Honda, O. Kitao, H. Nakai, M. Klene, X. Li, J.E. Knox, H.P. Hratchian, J.B. Cross, C. Adamo, J. Jaramillo, R. Gomperts, R.E. Stratmann, O. Yazyev, A.J. Austin, R. Cammi, C. Pomelli, J.W. Ochterski, P.Y. Ayala, K. Morokuma, G.A. Voth, P. Salvador, J.J. Dannenberg, V.G. Zakrzewski, S. Dapprich, A.D. Daniels, M.C. Strain, O. Farkas, D.K. Malick, A.D. Rabuck, K. Raghavachari, J.B. Foresman, J.V. Ortiz, Q. Cui, A.G. Baboul, S. Clifford, J. Cioslowski, B.B. Stefanov, G. Liu, A. Liashenko, P. Piskorz, I. Komaromi, R.L. Martin, D.J. Fox, T. Keith, M.A. Al- Laham, C.Y. Peng, A. Nanayakkara, M. Challacombe, P.M.W. Gill, B. Johnson, W. Chen, M.W. Wong, C. Gonzalez, J.A. Pople, GAUSSIAN 03, Revision C.02, Gaussian Inc., Wallingford, CT, 2004.
[31] T.H. Dunning Jr., J. Chem. Phys. 90 (1989) 1007.
[32] M. Westerhausen, B. Rademacher, W. Poll, J. Organomet. Chem. 421 (1991) 175.
[33] COLLECT, Data Collection Software, Nonius B.V., Netherlands, 1998.
[34] Processing of X-ray diffraction data collected in oscillation mode, in: Z. Otwinowski, W. Minor, C.W. Carter, R.M. Sweet (Eds.), Methods in Enzymology, Macromolecular Crystallography, Part A, vol. 276, Academic Press, 1997, pp. 307–326.
[35] G.M. Sheldrick, Acta Crystallogr. Sect. A 46 (1990) 467.
[36] G.M. Sheldrick, SHELXL-97 (Release 97-2), University of Göttingen, Germany, 1997.